Research Square

Preprints are preliminary reports that have not undergone peer review.
They should not be considered conclusive, used to inform clinical practice,
or referenced by the media as validated information.

Peatland climate-methane feedbacks in warming periods were governed by pH and hydrology

Megan Jenkins

an19796@bristol.ac.uk

University of Bristol https://orcid.org/0009-0002-4262-2441

Amelia Oakeshott

University of Bristol

Mike Vreeken

University of Bristol

Yiming Zhang

University of Bristol https://orcid.org/0000-0002-9502-5096

Toby Halamka

University of Bristol

Simon Cheung

University of Bristol https://orcid.org/0000-0002-2764-2113

Caroline Signori-Müller

https://orcid.org/0000-0003-1047-1896

Ana Abrahamsen

University of Exeter

Paola Alarcon Prado

University of Bristol

Florence Schubotz

University of Bremen https://orcid.org/0000-0002-5680-1734

Juan Benavides

Pontificia Universidad Javeriana https://orcid.org/0000-0002-9694-2195

Frank Kansiime

Department of Environmental Management, Makerere University

Ellen Kayendeke

Department of Environmental Management, Makerere University

Carol Kagaba Kairumba

Wetlands Management Department, Ministry of Water and Environment,

Angela Gallego-Sala

University of Exeter https://orcid.org/0000-0002-7483-7773

Bernhard Naafs

University of Bristol https://orcid.org/0000-0001-5125-6928

Casey Bryce

University of Bristol https://orcid.org/0000-0002-1132-5201

Richard Pancost

University of Bristol https://orcid.org/0000-0003-0298-4026

Article

Keywords:

Posted Date: November 2nd, 2026

DOI: https://doi.org/10.21203/rs.3.rs-11037604/v1

License: This work is licensed under a Creative Commons Attribution 4.0 International License.
Read Full License

Additional Declarations: There is **NO** Competing Interest.

Peatland climate-methane feedbacks in warming periods were governed by pH and hydrology

M. Jenkins[1,2*], A. Oakeshott[1], M. Vreeken[1,2], Y. Zhang[1,2], T.A. Halamka[1,2], S.M.K. Cheung[1], C. Signori Muller[3], A. Abrahamsen[3], P. Alarcon Prado[2,4], F. Schubotz[5], J.C. Benavides[4], F. Kansiime[6], E. Kayendeke[6], C. Kagaba Kairumba[7], A. Gallego-Sala[3], B.D.A. Naafs[2], C. Bryce[1], R. Pancost[1,2]

[1] School of Earth Sciences, Cabot Institute for the Environment, University of Bristol, Bristol, BS8 1RJ, United Kingdom

[2] Organic Geochemistry Unit, Schools of Chemistry, Cabot Institute for the Environment, University of Bristol, Bristol, BS8 1TS, United Kingdom

[3] Department of Geography, College of Life and Environmental Sciences, University of Exeter, Exeter, EX4 4QE, United Kingdom

[4] Department of Ecology and Territory, Pontificia Universidad Javeriana, Bogota, 110231, Colombia

[5] MARUM Center for Marine Environmental Sciences and Department of Geosciences, University of Bremen, D-28359, Bremen, Germany

[6] Department of Environmental Management, Makerere University, Kampala, P.O. Box 7298, Uganda

[7] Wetlands Management Department, Ministry of Water and Environment, Kampala, P.O. Box 20026, Uganda

Materials and Correspondence: Megan Jenkins, an19796@bristol.ac.uk

Abstract

Methane is emitted naturally from peatlands, but controls on those emissions and their response to global warming remain debated. Previous research attempted to assess this by exploring how methane cycling responded to past warming events, with lipid biomarker signatures for methanotrophy (the ^{13}C-depletion of bacterially-derived hopanoids, $\delta^{13}C_{hop}$) revealing changes to the methane cycle during the Paleocene–Eocene Thermal Maximum (PETM). However, the lack of modern analogues has hindered interpretation of those changes. We present new $\delta^{13}C_{hop}$ data from a suite of tropical peatlands, including the discovery of exceptionally ^{13}C-depleted hopanoids, with values approaching those of the PETM. Across all sites, $\delta^{13}C_{hop}$ decreases with increasing pH, likely co-occurring with a shift from predominantly hydrogenotrophic to acetoclastic methanogenesis pathways. Modern sites with the lowest $\delta^{13}C_{hop}$ have elevated methane emissions, higher Type I to Type II methanotroph ratios, and higher methanogen proportions, linking hopanoid isotopic depletion to enhanced methane production and flux. These insights allow re-evaluation of geological records, with low PETM $\delta^{13}C_{hop}$ also indicating intensified peatland methane emissions. Such processes

evidently acted as positive feedbacks in the past and could do so in the future – not only as a direct response to warming but indirectly via changes to peatland hydrology and geochemistry.

Main

We must improve our understanding of how climate change impacts biogeochemical processes, especially greenhouse gas emissions.[1-3] Peatlands are of particular interest since they are massive carbon sequestration sites,[4,5] but also large natural sources of atmospheric methane – both today[6,7] and over the past ~400 Myrs.[8] This methane exerts a strong influence on Earth's radiative budget and hence global temperature,[6,9] yet our ability to anticipate future changes in peatland methane emissions is limited by the complexity of the methane cycle. Emissions are governed by the interplay between methane oxidation and production, both of which are sensitive to environmental changes, including temperature, hydrology, vegetation, and pH.[10,11] Higher temperatures can enhance peatland methane emissions due to elevated microbial metabolism, but climate-based differences in peatland hydrology and vegetation can simultaneously either reduce or amplify those emissions.[12-15]

Key insights into future biogeochemical responses to global warming can be revealed by their past responses.[16] The Palaeocene-Eocene Thermal Maximum (PETM) has been a focus for such investigations, including several that indicate a profound change in peatland[17-20] and lacustrine methane cycling.[21] Such findings complement Earth System modelling studies that suggest methane played a key role in driving global temperatures during greenhouse periods.[22,23] Pancost et al. (2007) first observed a significant decrease in the $\delta^{13}C$ of bacterial derived hopanoids across the (onset of the) PETM in the Cobham Lignite, which indicated a dramatic increase in the proportion of methanotrophic vs heterotrophic hopanoid-producing bacteria (HPB).[24] This finding has been recently replicated, with similar depleted hopanoid $\delta^{13}C$ found in lignites from the PETM of New Zealand (Inglis et al. 2020), the PETM and adjacent intervals in the high Arctic,[18-20] and the PETM and other Eocene hyperthermals in NE China.[20]

Unfortunately, the lack of modern analogues for these ^{13}C-depleted hopanoids[25] has precluded a mechanistic understanding of past perturbations or even their interpretation as positive or negative feedbacks. A stronger methanotroph signature could be a response to increased methane production, associated with greater methane emissions, or hydrological changes that favour methanotrophic consumption of a stable methane flux, causing a decrease in methane.[26] As such, we lack a functional insight of what depleted hopanoid $\delta^{13}C$ values in the geological past mean in terms of methane emissions and climate feedbacks. To address this gap, we extended the existing modern database of peatland hopanoid $\delta^{13}C$ values,[25] discovered low hopanoid $\delta^{13}C$ values, and interpret them in the context of environmental conditions, microbiological profiling, and methane emissions. We then revisit previous PETM sections, reinterpreting them in the context of our modern observations.

A global perspective on wetland hopane/ene stable carbon isotopic compositions

We expanded the Inglis et al. (2019) dataset with additional data from Amariei (2024) and eight new sites, focusing on adding a global distribution of low-lying tropical sites (Table 1, Supplementary Fig. 1 and Supplementary Excel A). We discuss these data as a single global dataset, but downcore bulk peat characteristics are shown for the eight new sites only (Supplementary Fig. 2). Hopanoids are biosynthesized by a wide range of bacteria, both hetero- and methanotrophs.[27] The balance between these two metabolisms can be qualified using stable hopanoid $\delta^{13}C$ values[25] with values < -50‰ often representing incorporation of ^{13}C-depleted methane,[28,29] and values > -50‰ likely having a more heterotrophic origin. As hopanoids exist as different forms in wetlands,[30,31] we focus on the most abundant components: short-chain (< C_{30}) hopanes/enes, C_{31} αβ hopanoids, and C_{31} ββ hopanoids, with a strong emphasis on the $\delta^{13}C$ of hop-22(29)-ene (diploptene).

Table 1. New Study Sites, including acronyms, major vegetation, site coordinates, mean annual temperature (MAT), and pH (further data in SI).

Site	Acronym	Major Vegetation	Site Coordinates	MAT / ℃	pH
Colombia Amacayacu Cananguchal	CAC	*Mauritia flexuosa* L.f. (Arecaceae) palm	3°48'25.4"S 70°13'40.3"W	26	5.4
Colombia Amacayacu Pantano	CAP	*Montrichardia arborescens* (L.) Schott (Araceae)	3°48'50.5"S 70°16'03.5"W	26	6.6
Colombia Inírida	CIH	Hardwood trees	3°45'02.6"N 67°49'45.7"W	26	5.3
Panama Hardwood	SSPS2	*Raphia taedigera* & *Campnosperma panamensis*,	9°22'51.4"N 82°22'00.4"W	26	4.0
Panama Sawgrass	SSPS4	*Cladium mariscus*	9°23'01.5"N 82°21'57.7"W	26	4.0
United States, Everglades Lilypad	US_WCA1	*Nymphaea odorata* water lily	26°30'18.0"N 80°15'52.0"W	23	6.6
Uganda Papyrus (Mpologoma Peatland)	UMp_PA2	*Cyperus papyrus* (papyrus)	0°57'53.3"N 33°44'31.3"E	20	6.6
UK Ombrotrophic Bog (Tor Royal)	UKTR_1	*Sphagnum* with some sedge	50°32'08.4"N 3°58'15.5"W	8.1	4.8

A range of hopanes/enes were identified (Supplementary Fig. 3). In our global database, hop-22(29)-ene (diploptene) had an average $\delta^{13}C_{dip}$ of -36.0‰, but a large range of -23.0 to -57.0‰. Crucially, the lowest diploptene $\delta^{13}C$ values were >10‰ depleted relative to all previous reported hopanoids from any modern peatland and occurred at the Colombian Amacayacu Pantano Swamp (CAP; up to -56.7‰). Low values (up to -42.4‰) also occurred in the Mpologoma Papyrus Swamp (UMp_PA2),

despite the dominance of C4 vegetation (Supplementary Fig. 4). The average C_{31} αβ hopane (22R stereoisomer) $\delta^{13}C$ was -26.8‰, with a range of -17.0 to -35.0‰. As previously observed, C_{31} hopanes were frequently ^{13}C-enriched relative to *n*-alkanes, likely due to preferential heterotrophic consumption of ^{13}C-enriched substrates.[24,26] Consequently, across all sites, C_{31} αβ (and ββ) hopane $\delta^{13}C$ values were almost always enriched in ^{13}C compared with diploptene (Supplementary Fig. 4), and diploptene exhibited the greatest variability.

This observation is consistent with previous studies (Inglis et al., 2019) indicating that diploptene is the most sensitive to changes in the balance between heterotrophic and methanotrophic bacteria. The ratio of diploptene to C_{31} hopane abundance (all isomers) increases with pH (R^2 = 0.48, $p << 0.01$; Supplementary Fig. 5) and hopanoid ^{13}C-depletion (R^2 = 0.42, $p << 0.01$; Supplementary Fig. 5), confirming enhanced production of diploptene where stronger methanotrophy signals are observed, rather than diminished heterotrophic production. This is consistent with diploptene being derived from a wide range of bacteria, including methanotrophs.[32] In contrast, C_{31} hopanes have lower methanotroph contributions as they derive from the degradation of tetrafunctionalised BHPs, but diagnostic methanotroph BHPs are penta- and hexa-functionalised.[33]

Heterotrophs comprise a significant part of the peat HPB community,[34] and changes in substrate can drive hopanoid $\delta^{13}C$ values without a change in the methanotroph/heterotroph balance.[24,25,29] This is especially true for the Ugandan Papyrus Swamp, which features C_4 vegetation. Corrections are done using either plant-derived biomarkers (leaf wax *n*-alkanes) or bulk organic matter: $\Delta^{13}C = \delta^{13}C_{hopanoid} - \delta^{13}C_{alk/TOC}$.[25] To explore which *n*-alkane provides the greatest fidelity for representing bulk organic matter, we compared $\delta^{13}C_{alk}$ and $\delta^{13}C_{TOC}$ for the new sites (see supplementary information, section 4, and Supplementary Figs. 6, 7). Based on that analysis, we report hopanoid $\delta^{13}C$ values as offsets relative to *n*-C_{27} to maximise consistency with previously published data; the exception is the peatland dominated by C_4 plants, for which we use *n*-C_{23}. The average diploptene values corrected for biomass ($\Delta^{13}C_{dip\text{-}alk}$) were -3.8‰, ranging from -20 to +9‰, whereas the average C_{31} αβ hopane (22R) $\Delta^{13}C_{hop\text{-}alk}$ value was higher (+6.1‰) with a narrower range of -2 to +16‰. Trends among sites are consistent with unadjusted $\delta^{13}C$ values, apart from the Ugandan Papyrus Swamp, where the correction for ^{13}C-enriched C_4 vegetation yields a strong 14.6‰ depletion in $\delta^{13}C_{diploptene}$ relative to peat biomass.

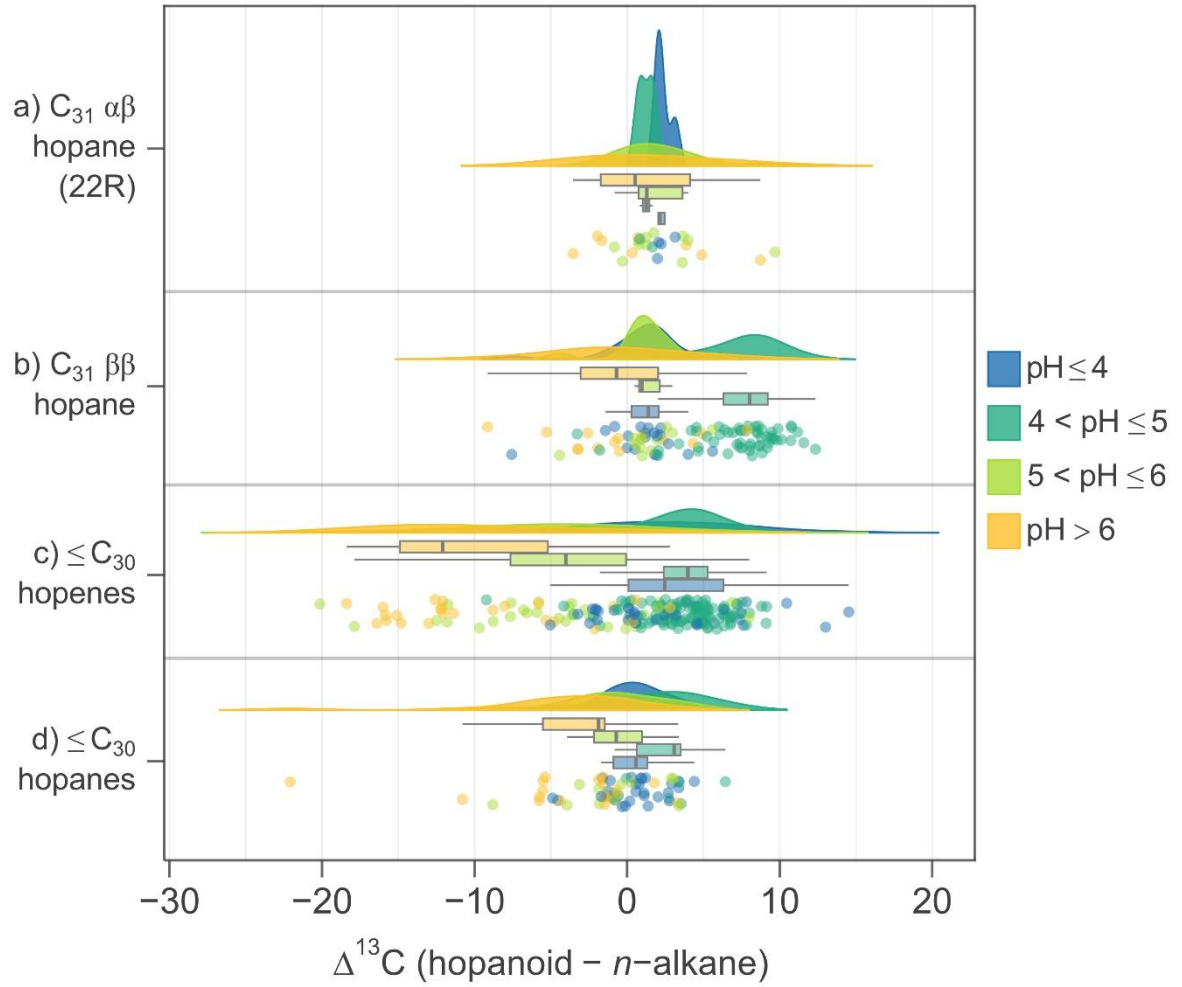


Figure 1. The variation of modern $\Delta^{13}C_{hopanoid\text{-}n\text{-}alkane}$ between peatlands with pH across the top 100 cm. The spread of $\Delta^{13}C_{hopanoid\text{-}n\text{-}alkane}$ for a) C_{31} αβ 22R; b) C_{31} ββ; c) ≤C_{30} hopenes; and d) ≤C_{30} hopanes across peatlands are grouped by observed (surface) pH; pH ≤ 4, dark blue, *n* = 40; 4 < pH ≤ 5, dark green, *n* = 91; 5 < pH ≤ 6, light green, *n* = 35; pH ≥ 6, yellow, *n* = 30. Data originate from different depths within the top 100 cm, and each depth from a single site is treated as a unique datapoint. The panel shows $\delta^{13}C_{hopanoid}$ corrected by the most appropriate $\delta^{13}C_{n\text{-}alkane}$ ($\Delta^{13}C_{hopanoid\text{-}n\text{-}alkane}$) as discussed in the supplementary information. Dots on the graph are data points and box plots show the spread of the (same) data for each category. For pH ≤ 4: C_{31} αβ 22R, *n* = 22; C_{31} ββ, *n* = 19; ≤C_{30} hopenes, *n* = 39; ≤C_{30} hopanes, *n* = 30. For 4 < pH ≤ 5: C_{31} αβ 22R, *n* = 74; C_{31} ββ, *n* = 56; ≤C_{30} hopenes, *n* = 104; ≤C_{30} hopanes, *n* = 6. For 5 < pH ≤ 6: C_{31} αβ 22R, *n* = 14; C_{31} ββ, *n* = 12; ≤C_{30} hopenes, *n* = 15; ≤C_{30} hopanes, *n* = 12. For pH > 6 4: C_{31} αβ 22R, *n* = 8; C_{31} ββ, *n* = 14; ≤C_{30} hopenes, *n* = 24; ≤C_{30} hopanes, *n* = 17.

For all hopanoids, sites with pH ≥ 5.5 had more negative and a larger spread of $\Delta^{13}C_{hop\text{-}alk}$ values (-20 to +3‰) than peatlands with a pH < 5 (-5 to +5‰) (Figs. 1, 2). The $\Delta^{13}C_{dip\text{-}alk}$ also became more negative with increasing pH (Fig. 2), with the lowest (average) $\Delta^{13}C_{dip\text{-}alk}$ occurring in three high pH, minerotrophic sites: the Peruvian Buena Vista forested peatland (Amariei, 2024; $\Delta^{13}C_{dip\text{-}alk}$ = -10.0‰, pH = 5.8) and the Uganda Papyrus and Colombia Amacayacu Pantano Swamps (-13.6 and -14.6‰ respectively, both with measured pH = 6.6). However, other sites with similar modern pH do not have

such depleted values. For example, in the Everglades Lilypad Swamp (pH 6.6), $\Delta^{13}C_{dip\text{-}alk}$ ranged between -8 and -5‰, indicating that pH is not the sole control on methanotroph abundances.

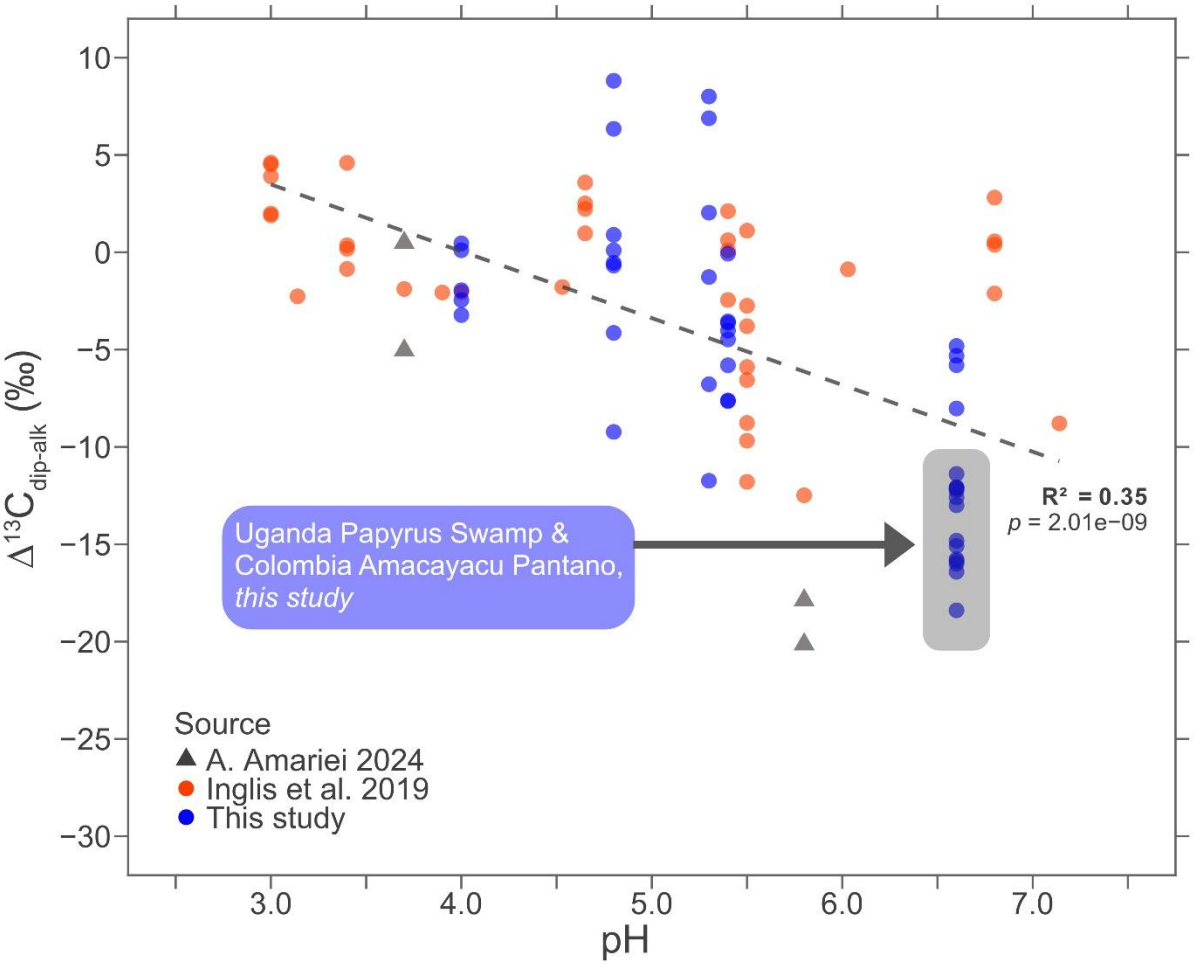


Figure 2. The variation of modern peatland $\Delta^{13}C_{dip\text{-}alk}$ with modern peatland pH. Crossplot of current peatland pH against $\Delta^{13}C_{dip\text{-}alk}$ for combined dataset (upper 100 cm, *n* = 86). Symbols/colours distinguish previously recorded (A. Amariei et al., 2024, *n* = 4, filled grey triangles), and previously published (Inglis et al., 2019, *n* = 37, filled red circles) from new data (This study, *n* = 45, filled blue circles). Most datapoints have been corrected with *n*-C_{27} except Ballyduff Bog, Ireland (Inglis et al. 2019; corrected with *n*-C_{29} since *n*-C_{27} was not determined) and the Uganda Papyrus Swamp (This study; corrected with *n*-C_{23} to reflect dominant vegetation). In places where *n*-C_{27} was absent for a particular sampling depth, the average of *n*-C_{27} across all depths at that site was used. A simple linear regression was calculated to determine R^2 and significance values.

Since our work suggests dramatic variations in peatland methanotroph communities, we used 16S rRNA sequence data at our new sites to explore the methane oxidising bacterial (MOB) community (Fig. 3, Supplementary Fig. 9). MOB represented a small portion of the bacterial community, having a relative abundance < 18%; however, MOB proportions exhibited the anticipated depth profiles, with their greatest proportion occurring at/near the peat surface and anticipated redox boundaries (Supplementary Fig. 9). Sites with the lowest $\Delta^{13}C_{dip\text{-}alk}$ values (Colombia Amacayacu Pantano and Uganda Papyrus Swamps) did not have highest MOB proportions, and we observe no significant relationship between $\Delta^{13}C_{dip\text{-}alk}$ and %MOB derived from 16S rRNA data (R^2 = 0.27, $p >> 0.05$). It is likely that peatland hopanoid $\Delta^{13}C_{dip\text{-}alk}$ values do not directly reflect relative 16S-derived MOB

abundance, since lipid biomarkers record an integrated signal over decadal timescales,[35] while 16S rRNA reflects much shorter timescales.

We also explored the specific methanotroph carbon assimilation pathway in these tropical peatlands, specifically the relative contribution of Type I and Type II methanotrophs.[12,36] Type II methanotrophs were always more abundant than Type I methanotrophs (Supplementary Fig. 9), consistent with previous studies that mainly focused on acidic and boreal peatlands (e.g.[37,38]). However, in the Colombia Amacayacu Pantano and Uganda Papyrus Swamps, sites with the lowest $\Delta^{13}C_{dip\text{-}alk}$, the proportions of Type I MOB within the total (Type I + II) MOB pool were higher, with maxima up to 36% compared to < 5% elsewhere; and Type I/ (Type I + II) ratios were negatively correlated to $\Delta^{13}C_{dip\text{-}alk}$ ($R^2 = 0.9$, $p << 0.01$; Supplementary Fig. 10). The differing carbon assimilation pathways of Type I and II MOB can lead to greater ^{13}C-depletion in Type I bacterial lipids compared to Type II MOB.[25,28,37] Thus, this shift in MOB community could contribute to (but is not large enough to fully explain) the larger $\Delta^{13}C_{dip\text{-}alk}$ offsets observed in the Colombia Amacayacu Pantano and Uganda Papyrus Swamps. Crucially, some studies suggest that Type I MOB are more abundant relative to Type II MOB in environments where methane- and nutrient-limitation is alleviated,[39,40] indicating that the sites with greater proportions of the former are characterised by nutrient-rich conditions and/or high methane fluxes.[40]

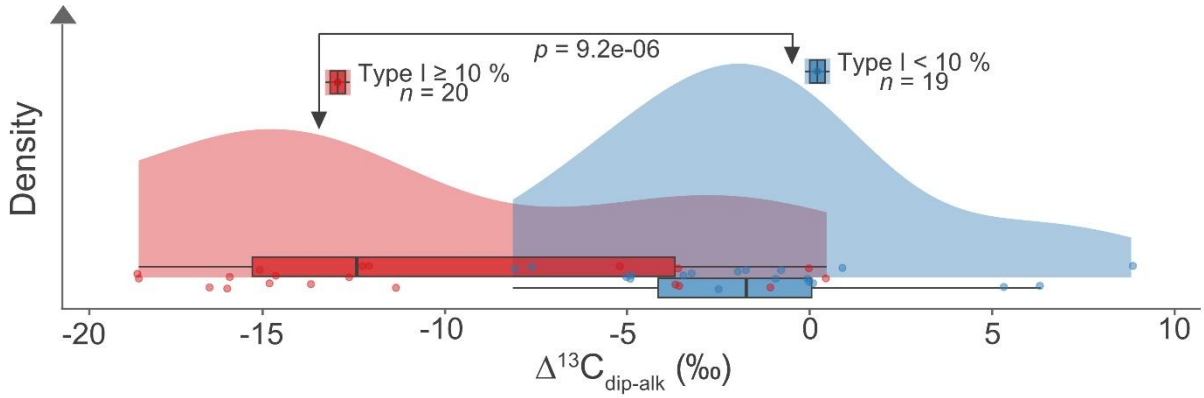


Figure 3. The variation in $\Delta^{13}C_{dip\text{-}alk}$ with % Type I of (Type I + II MOB) across peatlands from this study (CERES) only. The distribution of observed $\Delta^{13}C_{dip\text{-}alk}$ values corrected for vegetation with the most appropriate *n*-alkane (see Supplementary Figs. 6, 7). The data are colour-coded based on a 10% threshold for high (red) or low (blue) contributions of Type I MOB relative to total Type I + II MOB, based on 16S rRNA sequence analysis. 16S rRNA data was only available for the new data and not previously analysed sites. The plot shows data from across the top 100 cm of peat cores from this study only and treats each depth as a unique datapoint since methanotroph and Type I MOB abundances vary dramatically with depth reflecting requirements for both methane and oxygen. No microbiology data was available for Colombia Inirida Hardwood, so this is not included in figure 3. The percentages used to define each grouping are arbitrary and based on the average % of Type I MOB across the top 100 cm of this dataset. The box plots show the spread of the data for above and below the mean of total Type I MOB %, and the mean of each grouping is also indicated by the respective box plot.

Causes of hopanoid ^{13}C-depletion in some peatlands

The tropical (and high pH) Peruvian Buena Vista Hardwood, Ugandan Papryus and Colombia Amacayacu Pantano swamps are the first modern peatland analogues for past global change events that feature strikingly ^{13}C-depleted hopanoids. This depletion likely reflects a larger MOB community,

188 despite the lack of a clear signal in the 16S rRNA community analysis, enhanced by higher
189 abundances of Type I methanotrophs.[28] High temperatures directly stimulate methanotrophy,[41-43] but
190 we do not observe ^{13}C-depleted hopanoids at all tropical peatland sites, and MAT is poorly related to
191 $\Delta^{13}C_{dip\text{-}alk}$ ($R^2 = 0.1$, $p << 0.01$; Supplementary Fig. 8). Instead, hopanoid evidence for methanotrophy
192 appears to be a response to higher methane flux, consistent with previous experimental studies.[44]
193 Tropical peatlands have higher CH_4 emissions compared with temperate peatlands,[13] reflecting high
194 rates of CH_4 production[45-47] that would fuel methanotrophic growth. Confirming this, CH_4 fluxes from
195 the Peruvian Buena Vista, Colombia Amacayacu Pantano and Uganda Papyrus swamps are notably
196 higher than sites with heavier $\Delta^{13}C_{dip\text{-}alk}$, and they are high emission end-members among global
197 peatlands (Supplement Section 7).[48] Higher proportions of Type I to Type II MOB relative abundances
198 are also consistent with these peatlands being high methane flux environments.[40] Maintaining
199 elevated methane emissions despite inferred greater methanotrophic activity requires high methane
200 production rates, suggesting larger methanogen populations; and proportions of methanogens from
201 our new sites, derived from 16S rRNA are consistent with this (Supplementary Figs. 9,11).

202 Methane production, therefore, is almost certainly the primary control on hopanoid ^{13}C-depletion, and
203 this provides a mechanism for the strong correlation between depletion and pH (Fig. 2). Typically,
204 acidic and nutrient-poor peatlands are dominated by hydrogenotrophic methanogenesis, whereas
205 acetoclastic methanogens dominate in minerotrophic and high pH settings,[49,50] with the latter
206 associated with higher rates of methanogenesis and greater methane emissions.[51,52] Hopanoid $\delta^{13}C$
207 values have not been corrected for CH_4 $\delta^{13}C$, but doing so would yield the opposite trend to that
208 observed; the dominance of acetoclastic over hydrogenotrophic methanogenesis at high pH would
209 cause higher rather than lower hopanoid $\delta^{13}C$ values.[53] Instead, greater abundances of
210 methanotrophic HPB inferred from $\Delta^{13}C_{dip\text{-}alk}$ in high pH settings reflect the higher rates of methane
211 production. This also explains why some high pH sites, like the Everglades Lilypad Swamp, have low
212 $\Delta^{13}C_{dip\text{-}alk}$ values; it is nitrate-rich due to agricultural contamination,[54] which likely suppressed
213 methanogenesis.[55]

214 Although high pH appears to be a pre-condition for strong biomarker signatures for methanotrophy,
215 many high pH sites do not exhibit them (Fig. 2), indicating the importance of other factors, such as
216 vegetation and hydrology.[48] Higher water table levels (WTL) in tropical peatlands promote anoxic
217 conditions, enhancing methanogenic activity and methane production.[46,56] Many of our tropical sites
218 are characterized by high WTLs, but the Buena Vista peatland,[57] Uganda Papyrus and Colombia
219 Amacayacu Pantano swamps are distinguished by being hydraulically associated with river systems
220 which result in persistently high but seasonally variable WTL (Supplementary Information Section 1).
221 Microbial community analysis confirms that the elevated WTLs support methanogen populations
222 throughout the peat profile at the latter two sites and especially at the surface (Supplementary Fig.11).
223 Moreover, association with rivers provides elevated nutrients for both plants and methanogens, and
224 Buena Vista[57] and our sites, are all minerotrophic. Increased nutrient supply promotes microbial
225 growth and reduces the lag time before the onset of methanogenesis, favouring both methanogenic
226 and methanotrophic processes.[58] Vegetation further influences peatland CH_4 production by stimulating

the microbial community through primary productivity and root exudates.[59] The Ugandan Papyrus and Colombian Amacayacu Pantano peatlands are dominated by two highly productive macrophytes that can reach up to 5 m and have well-developed root systems. For example, *Cyperus papyrus* can transport fresh organic carbon to deeper peat layers,[50,60] including methanogenic substrates such as acetate.[61] Consistent with this, higher methanogenic potentials and methane flux have been observed from rich and intermediate fens compared with poor fens,[62] with the former characterised by higher water table positions, nutrient availability, and pH.[63] Therefore, highly negative $\Delta^{13}C_{dip\text{-}alk}$ values in peatlands evidently reflect a methanotroph population fuelled by high methane production in hydrologically dynamic, nutrient-rich, high pH settings.

Implications for understanding past (and future) peatland methane feedbacks

To compare our modern dataset with ancient peatlands, we compiled all palaeoenvironmental records for which $\Delta^{13}C_{hop\text{-}alk}$ and reconstructed pH (see Supplementary Information A, and B section 8) are available (Fig. 4). The available data are limited to the PETM (Cobham and Otaio Gorge sections)[18,25] and the early/mid Holocene (Hongyuan and Hani peat).[64-67] We complement those with our modern sites, for depths deeper than 100 cm, reflecting the mid/late Holocene. The modern and ancient data are remarkably consistent, exhibiting a significant negative relationship between pH and $\Delta^{13}C_{hop\text{-}alk}$ (Fig. 4). These findings have major implications for previous and ongoing investigations of past changes in peatland methane cycling. Most importantly, our finding that ^{13}C-depleted hopanoids are associated with high methane production rates and methane emissions indicates that their occurrence in ancient peatlands[17,18,20] is also evidence of high methane production. This confirms that the peatland methane cycle acted as a positive feedback during past transient warming, at least at the studied PETM sites.

Our new modern observations also provide a mechanistic framework for understanding those past changes. With respect to the PETM, it is tempting to attribute changes in methane cycling to higher temperatures, given the widespread evidence of significant warming.[68,69] However, neither ancient (e.g. Inglis et al., 2020; Pancost, 2024) nor modern settings (this work) exhibit a strong relationship between temperature and $\Delta^{13}C_{hop\text{-}alk}$ (Supplementary Fig. 8). Instead, changes in methane cycling recorded by $\Delta^{13}C_{hop\text{-}alk}$ are driven across multiple timescales by the interaction of pH, vegetation, and hydrology. The decrease in $\Delta^{13}C_{hop\text{-}alk}$ values at the PETM co-occurs with a dramatic increase in pH at both Cobham[25] and Otaio Gorge (Fig. 4).[18] Remarkably, both are also associated with an apparent increase in the proportion of Type I methanotrophs,[70,71] confirming their analogous character to the Uganda and Colombian Pantano peatlands. Both PETM sequences are associated with changing hydroclimate, with sedimentological evidence at Cobham indicating increased flooding,[72,73] and climate simulations indicating that both regions were characterised by more extreme precipitation during the PETM.[74] Such factors have not been included in previous Earth system modelling efforts to reconstruct past terrestrial methane emissions (e.g.[23]) and their inclusion will likely exacerbate the methane emission feedbacks identified in those studies, given the geographically widespread

intensification of PETM extreme rainfall events.[74] In fact, intensification of extreme rainfall events and associated biogeochemical consequences[74] unites multiple observations of methane cycling perturbations in diverse settings across Mesozoic to Cenozoic timescales. For example, Sun et al. 2025,[21] observed a muted but clear depletion in hopanoids in a saline lake, attributed to alleviation of salinity by increased rainfall at the PETM onset.

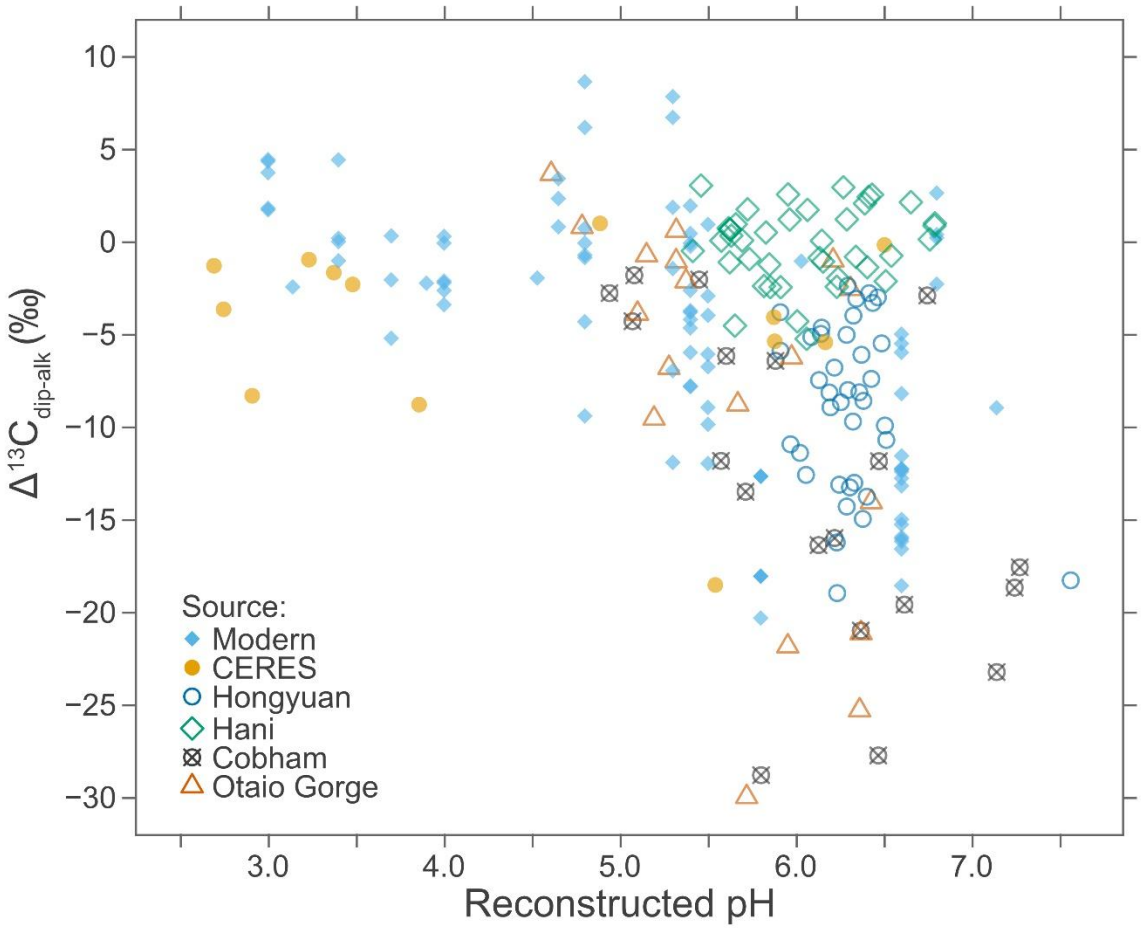


Figure 4. $\Delta^{13}C_{dip\text{-}alk}$ vs reconstructed pH in modern and ancient peat deposits. The ancient pH has been reconstructed using the CBT_{peat} index and the calibration $pH_{CBTpeat} = 9.19+(2.69*CBT_{peat})$,[75] for paleo peatlands. For the modern peatlands (lightly shaded blue diamonds), the measured pH has been used. The ancient data includes $\Delta^{13}C$ values for diploptene from sites from this study deeper than 100 cm (CERES sites, filled yellow circles, *n* = 14), the Hani peatland (Holocene, open green diamond, *n* = 41), the Hongyuan peatland (Holocene, open blue circle, *n* = 38) and the Cobham (open black circle with cross, *n* = 19) and Otaio Gorge Lignites (open orange triangle, *n* = 18) of PETM age.

These hydroclimate changes were globally widespread at the PETM[74] as well as other past hyperthermals – and could represent our future hot climate and associated rainfall extremes.[7] It is understood that future hydroclimate change will impact terrestrial methane emissions through peatland expansion or contraction, depending on overall water balance.[76] This work, by analogy with ancient warming events, confirms that future warming will also affect methane emissions through pH and hydrology-mediated changes in microbiology. Regions that experience increased hydroclimate-

induced changes in peatland connectivity to river systems appear particularly susceptible to experiencing enhanced methane emissions and acting as a positive feedback on global warming.

References

1 Bridgham, S. D., Pastor, J., Dewey, B., Weltzin, J. F. & Updegraff, K. Rapid Carbon Response of Peatlands to Climate Change. *Ecology* **89**, 3041-3048, doi:10.1890/08-0279.1 (2008).

2 Bridgham, S. D., Johnston, C. A., Pastor, J. & Updegraff, K. Potential Feedbacks of Northern Wetlands on Climate Change. *Bioscience* **45**, doi:DOI:10.2307/1312419 (1995).

3 Moore, T., Roulet, N. & Waddington, J. Uncertainty in predicting the effect of climatic change on the carbon cycling of Canadian peatlands. *Climatic Change* **40**, 229-245, doi:https://doi.org/10.1023/A:1005408719297 (1998).

4 Wang, S., Zhuang, Q., Lahteenoja, O., Draper, F. C. & Cadillo-Quiroz, H. Potential shift from a carbon sink to a source in Amazonian peatlands under a changing climate. *Proc Natl Acad Sci U S A* **115**, 12407-12412, doi:10.1073/pnas.1801317115 (2018).

5 Leifeld, J., Wüst-Galley, C. & Page, S. Intact and managed peatland soils as a source and sink of GHGs from 1850 to 2100. *Nature Climate Change* **9**, 945-947, doi:10.1038/s41558-019-0615-5 (2019).

6 Saunois, M. *et al.* The Global Methane Budget 2000–2017. *Earth System Science Data* **12**, 1561-1623, doi:10.5194/essd-12-1561-2020 (2020).

7 IPCC. IPCC, 2021: Climate Change 2021: The Physical Science Basis. Contribution of Working Group I to the Sixth Assessment Report of the Intergovernmental Panel on Climate Change. (2021).

8 Beerling, D., Berner, R. A., Mackenzie, F. T., Harfoot, M. B. & Pyle, J. A. Methane and the CH4 related greenhouse effect over the past 400 million years. *American Journal of Science* **309**, 97-113, doi:10.2475/02.2009.01 (2009).

9 IPCC. IPCC, 2013: Climate Change 2013: The Physical Science Basis. Contribution of Working Group I to the Fifth Assessment Report of the Intergovernmental Panel on Climate Change 1535 pp (2013).

10 Krumholz, L. R., Hollenback, J. L., Roskes, S. J. & Ringelberg, D. B. Methanogenesis and methanotrophy within a Sphagnum peatland. *FEMS Microbiol Ecol* **18**, 215 - 224, doi:10.1016/0168-6496(95)00061-4 (1995).

11 Tian, W. *et al.* Water table level controls methanogenic and methanotrophic communities and methane emissions in a Sphagnum dominated peatland. *Microbiology Spectrum* **11**, doi:https://doi.org/10.1128/spectrum.01992-23 (2023).

12 Hanson, R. S. & Hanson, T. E. Methanotrophic Bacteria. *Microbiol. Rev.* **60**, 439-471 (1996).

13 Dean, J. F. *et al.* Methane Feedbacks to the Global Climate System in a Warmer World. *Reviews of Geophysics* **56**, 207-250, doi:10.1002/2017rg000559 (2018).

14 Updegraff, K., Bridgham, S. D., Pastor, J., Weishampel, P. & Harth, C. Response of CO2 and CH4 emissions from Peatlands to Warming and Water Table Manipulation. *Ecological Applications* **11**, 311-326, doi:10.1890/1051-0761(2001)011[0311:Rocace]2.0.Co;2 (2001).

15 Limpens, J. *et al.* Peatlands and the carbon cycle: from local processes to global implications - a synthesis. *Biogeosciences* **5**, 1475-1491, doi:DOI:10.5194/bg-5-1475-2008 (2008).

16 Zachos, J. C., Dickens, G. R. & Zeebe, R. E. An early Cenozoic perspective on greenhouse warming and carbon-cycle dynamics. *Nature* **451**, 279-283, doi:10.1038/nature06588 (2008).

17 Pancost, R. D. *et al.* Increased terrestrial methane cycling at the Palaeocene-Eocene thermal maximum. *Nature* **449**, 332-335, doi:10.1038/nature06012 (2007).

18 Inglis, G. N. *et al.* Terrestrial methane cycle perturbations during the onset of the Paleocene-Eocene Thermal Maximum. *Geology* **49**, 520-524, doi:10.1130/g48110.1 (2020).

19 Blumenberg, M. *et al.* Biomarker Reconstruction of a High-Latitude Late Paleocene to Early Eocene Coal Swamp Environment Across the PETM and ETM-2 (Ellesmere Island, Arctic Canada). *Paleoceanography and Paleoclimatology* **39**, doi:10.1029/2023pa004712 (2024).

20 Chen, Z. *et al.* Wetland methane feedback during the early Eocene hyperthermals. *Geology* **53**, 404-408, doi:10.1130/g52899.1 (2025).

21 Sun, F. *et al.* Salinity limited methane cycling in lacustrine settings during the Paleocene–Eocene Thermal Maximum. *Geology* **54**, 50-54, doi:10.1130/g53790.1 (2025).

22 Sloan, L. C., Walker, J. C. G., Moore, T. C., Rea, D. K. & Zachos, J. C. . Possible methane-induced polar warming in the early Eocene. *Nature* **357**, 320-322, doi:10.1038/357320a0 (1992).

23 Beerling, D. J., Fox, A., Stevenson, D. S. & Valdes, P. J. Enhanced chemistry-climate feedbacks in past greenhouse worlds. *Proc Natl Acad Sci U S A* **108**, 9770-9775, doi:10.1073/pnas.1102409108 (2011).

24 Pancost, R. D. & Sinninghe Damsté, J. S. Carbon isotopic compositions of prokaryotic lipids as tracers of carbon cycling in diverse settings. *Chemical Geology* **195**, 29-58, doi:10.1016/s0009-2541(02)00387-x (2003).

25 Inglis, G. N., Naafs, B. D. A., Zheng, Y., Schellekens, J. & Pancost, R. D. δ13C values of bacterial hopanoids and leaf waxes as tracers for methanotrophy in peatlands. *Geochimica et Cosmochimica Acta* **260**, 244-256, doi:10.1016/j.gca.2019.06.030 (2019).

26 Pancost, R. D. Biomarker carbon and hydrogen isotopes reveal changing peatland vegetation, hydroclimate and biogeochemical tipping points. *Quaternary Science Reviews* **339**, doi:10.1016/j.quascirev.2024.108828 (2024).

27 Talbot, H. M., Rohmer, M. & Farrimond, P. Rapid structural elucidation of composite bacterial hopanoids by atmospheric pressure chemical ionisation liquid chromatography/ion trap mass spectrometry. *Rapid Commun Mass Spectrom* **21**, 880-892, doi:10.1002/rcm.2911 (2007).

28 Jahnke, L. L., Summons, R. E., Hope, J. M. & Des Marais, D. J. Carbon isotopic fractionation in lipids from methanotrophic bacteria II: The effects of physiology and environmental parameters on the biosynthesis and isotopic signatures of biomarkers. *Geochimica et Cosmochimica Acta* **63** (1999).

29 Pancost, R. D., van Geel, B., Baas, M. & Sinninghe Damsté, J. S. δ13C values and radiocarbon dates of microbial biomarkers as tracers for carbon recycling in peat deposits. *Geology* **28**, 663-666, doi:DOI:10.1130/0091-7613(2000)28<663:CVARDO>2.0.CO (2000).

30 Mackenzie, A. S., Patience, R. L., Maxwell, J. R., VandenBroucke, M. & Durand, B. Molecular parameters of maturation in the Toarcian shales, Paris Basin, France-I. Changes in the configurations of acyclic isoprenoid alkanes, steranes and triterpanes *Geochimica et Cosmochimica Acta* **44**, 1709-1721 (1980).

31 Inglis, G. N. *et al.* Distributions of geohopanoids in peat: Implications for the use of hopanoid-based proxies in natural archives. *Geochimica et Cosmochimica Acta* **224**, 249-261, doi:10.1016/j.gca.2017.12.029 (2018).

32 Belin, B. J. *et al.* Hopanoid lipids: from membranes to plant-bacteria interactions. *Nat Rev Microbiol* **16**, 304-315, doi:10.1038/nrmicro.2017.173 (2018).

33 Kusch, S. & Rush, D. Revisiting the precursors of the most abundant natural products on Earth: A look back at 30+ years of bacteriohopanepolyol (BHP) research and ahead to new frontiers. *Organic Geochemistry* **172**, doi:10.1016/j.orggeochem.2022.104469 (2022).

34 Xie, S. *et al.* Concordant monsoon-driven postglacial hydrological changes in peat and stalagmite records and their impacts on prehistoric cultures in central China. *Geology* **41**, 827-830, doi:10.1130/g34318.1 (2013).

35 Wormer, L. *et al.* Ultra-high-resolution paleoenvironmental records via direct laser-based analysis of lipid biomarkers in sediment core samples. *Proc Natl Acad Sci U S A* **111**, 15669-15674, doi:10.1073/pnas.1405237111 (2014).

36 Trotsenko, Y. A. & Murrell, J. C. Metabolic aspects of aerobic obligate methanotrophy. *Adv Appl Microbiol* **63**, 183-229, doi:10.1016/S0065-2164(07)00005-6 (2008).

37 Dedysh, S. N. Exploring methanotroph diversity in acidic northern wetlands: Molecular and cultivation-based studies. *Microbiology* **78**, 655-669, doi:10.1134/s0026261709060010 (2009).

38 Dedysh, S. N., Derakshani, M. & Liesack, W. Detection and enumeration of methanotrophs in acidic Sphagnum peat by 16S rRNA fluorescence in situ hybridization, including the use of newly developed oligonucleotide probes for Methylocella palustris. *Appl Environ Microbiol* **67**, 4850-4857, doi:10.1128/AEM.67.10.4850-4857.2001 (2001).

39 Cai, Y., Zheng, Y., Bodelier, P. L., Conrad, R. & Jia, Z. Conventional methanotrophs are responsible for atmospheric methane oxidation in paddy soils. *Nat Commun* **7**, 11728, doi:10.1038/ncomms11728 (2016).

40 Ho, A. *et al.* Conceptualizing functional traits and ecological characteristics of methane-oxidizing bacteria as life strategies. *Environ Microbiol Rep* **5**, 335-345, doi:10.1111/j.1758-2229.2012.00370.x (2013).

41 Mohanty, S. R., Bodelier, P. L. & Conrad, R. Effect of temperature on composition of the methanotrophic community in rice field and forest soil. *FEMS Microbiol Ecol* **62**, 24-31, doi:10.1111/j.1574-6941.2007.00370.x (2007).

42 King, G. Responses of atmospheric methane consumption by soils to global climate change. *Global Change Biology* **3**, 351-362, doi:10.1046/j.1365-2486.1997.00090.x (1997).

43 Kip, N. *et al.* Global prevalence of methane oxidation by symbiotic bacteria in peat-moss ecosystems. *Nature Geoscience* **3**, 617-621, doi:10.1038/ngeo939 (2010).

44 van Winden, J. F. *et al.* Influence of temperature on the delta(13) C values and distribution of methanotroph-related hopanoids in Sphagnum-dominated peat bogs. *Geobiology* **18**, 497-507, doi:10.1111/gbi.12389 (2020).

45 Segers, R. Methane production and methane consumption: a review of processes underlying wetland methane fluxes. *Biogeochemistry* **41**, 23-51 (1998).

46 van Winden, J. F., Reichart, G. J., McNamara, N. P., Benthien, A. & Damste, J. S. Temperature-induced increase in methane release from peat bogs: a mesocosm experiment. *PLoS One* **7**, e39614, doi:10.1371/journal.pone.0039614 (2012).

47 Yvon-Durocher, G. *et al.* Methane fluxes show consistent temperature dependence across microbial to ecosystem scales. *Nature* **507**, 488-491, doi:10.1038/nature13164 (2014).

48 Abrahamsen, A. *et al.* Exceptional methane emissions from an African papyrus wetland. *Research Square, Version 1.*, doi:10.21203/rs.3.rs-10680330/v1 (submitted).

49 Kotsyurbenko, O. R. *et al.* shift from acetoclastic to H2-dependent methanogenesis in a west Siberian peat bog at low pH values and isolation of an acidophilic Methanobacterium strain. *Appl Environ Microbiol* **73**, 2344-2348, doi:10.1128/AEM.02413-06 (2007).

50 Galand, P. E., Fritze, H., Conrad, R. & Yrjala, K. Pathways for methanogenesis and diversity of methanogenic archaea in three boreal peatland ecosystems. *Appl Environ Microbiol* **71**, 2195-2198, doi:10.1128/AEM.71.4.2195-2198.2005 (2005).

51 Kusin, K. *et al.* Increasing the pH of tropical peat can enhance methane production and methanogenic growth under anoxic conditions. *Catena* **250**, doi:10.1016/j.catena.2025.108791 (2025).

52 Ye, R. *et al.* pH controls over anaerobic carbon mineralization, the efficiency of methane production, and methanogenic pathways in peatlands across an ombrotrophic–minerotrophic gradient. *Soil Biology and Biochemistry* **54**, 36-47, doi:10.1016/j.soilbio.2012.05.015 (2012).

53 Hornibrook, E. R. C., Longstaffe, F. J. & Fyfe, W. S. Spatial distribution of microbial methane production pathways in temperate zone wetland soils: Stable carbon and hydrogen isotope evidence. *Geochimica et Cosmochimica Acta* **61**, 745-753, doi:https://doi.org/10.1016/S0016-7037(96)00368-7 (1997).

54 Wright, A. L., R, R. K. & Newman, S. Biogeochemical Response of the Everglades Landscape to Eutrophication *Global J. Environ. Res.,* **2**, 102-109 (2008).

55 Conrad, R. Importance of hydrogenotrophic, aceticlastic and methylotrophic methanogenesis for methane production in terrestrial, aquatic and other anoxic environments: A mini review. *Pedosphere* **30**, 25-39, doi:10.1016/s1002-0160(18)60052-9 (2020).

56 Blodau, C., Basiliko, N. & Moore, T. R. Carbon turnover in peatland mesocosms exposed to different water table levels. *Biogeochemistry* **67**, 331-351 (2004).

57 Lähteenoja, O., Ruokolainen, K., Schulman, L. & Alvarez, J. Amazonian floodplains harbour minerotrophic and ombrotrophic peatlands. *Catena* **79**, 140-145, doi:10.1016/j.catena.2009.06.006 (2009).

58 Finn, D. R. *et al.* Methanogens and Methanotrophs Show Nutrient-Dependent Community Assemblage Patterns Across Tropical Peatlands of the Pastaza-Maranon Basin, Peruvian Amazonia. *Front Microbiol* **11**, 746, doi:10.3389/fmicb.2020.00746 (2020).

59 Freitag, T. E., Toet, S., Ineson, P. & Prosser, J. I. Links between methane flux and transcriptional activities of methanogens and methane oxidizers in a blanket peat bog. *FEMS Microbiol Ecol* **73**, 157-165, doi:10.1111/j.1574-6941.2010.00871.x (2010).

60 Schimel, J. P. Plant transport and methane production as controls on methane flux from arctic wet meadow tundra. *Biogeochemistry* **28**, 183-200 (1995).

61 Ström, L., Mastepanov, M. & Christensen, T. R. Species-specific Effects of Vascular Plants on Carbon Turnover and Methane Emissions from Wetlands. *Biogeochemistry* **75**, 65-82, doi:10.1007/s10533-004-6124-1 (2005).

62 Zhang, H. *et al.* Methane production and oxidation potentials along a fen-bog gradient from southern boreal to subarctic peatlands in Finland. *Glob Chang Biol* **27**, 4449-4464, doi:10.1111/gcb.15740 (2021).

63 Lai, D. Y. F. Methane Dynamics in Northern Peatlands: A Review. *Pedosphere* **19**, 409-421, doi:https://doi.org/10.1016/S1002-0160(09)00003-4 (2009).
64 Zheng, Y. *et al.* Peatland GDGT records of Holocene climatic and biogeochemical responses to the Asian Monsoon. *Organic Geochemistry* **87**, 86-95, doi:10.1016/j.orggeochem.2015.07.012 (2015).
65 Zheng, Y. *et al.* Holocene variations in peatland methane cycling associated with the Asian summer monsoon system. *Nat Commun* **5**, 4631, doi:10.1038/ncomms5631 (2014).
66 Yang, H. *et al.* Different environmental controls on archaeal and bacterial GDGT distributions in Chinese peatlands. *Organic Geochemistry* **215**, doi:10.1016/j.orggeochem.2026.105174 (2026).
67 Huang, X. *et al.* Environmental factors affecting the low temperature isomerization of homohopanes in acidic peat deposits, central China. *Geochimica et Cosmochimica Acta* **154**, 212-228, doi:10.1016/j.gca.2015.01.031 (2015).
68 Tierney, J. E. *et al.* Spatial patterns of climate change across the Paleocene-Eocene Thermal Maximum. *Proc Natl Acad Sci U S A* **119**, e2205326119, doi:10.1073/pnas.2205326119 (2022).
69 Zachos, J. C. *et al.* Extreme warming of mid-latitude coastal ocean during the Paleocene-Eocene Thermal Maximum: Inferences from TEX86 and isotope data. *Geology* **34**, doi:10.1130/g22522.1 (2006).
70 Hollingsworth, E. H. *et al.* Bacteriohopanepolyols reveal a methane cycle perturbation during the Paleocene-Eocene Thermal Maximum. *Geochimica et Cosmochimica Acta* **426**, 14-27, doi:10.1016/j.gca.2026.06.001 (2026).
71 Talbot, H. M., McClymont, E. L., Inglis, G. N., Evershed, R. P. & Pancost, R. D. Origin and preservation of bacteriohopanepolyol signatures in Sphagnum peat from Bissendorfer Moor (Germany). *Organic Geochemistry* **97**, 95-110, doi:10.1016/j.orggeochem.2016.04.011 (2016).
72 Steart, D., Collinson, M., Scott, A., Glasspool, I. & Hooker, J. The Cobham Lignite Bed: the palaeobotany of two petrographically contrasting lignites from either side of the Paleocene–Eocene carbon isotope excursion. *Acta Palaeobotanica* **47**, 109-125 (2007).
73 Collinson, M. E. *et al.* Palynological evidence of vegetation dynamics in response to palaeoenvironmental change across the onset of the Paleocene-Eocene Thermal Maximum at Cobham, Southern England. *Grana* **48**, 38-66, doi:10.1080/00173130802707980 (2009).
74 Carmichael, M. J., Pancost, R. D. & Lunt, D. J. Changes in the occurrence of extreme precipitation events at the Paleocene–Eocene thermal maximum. *Earth and Planetary Science Letters* **501**, 24-36, doi:10.1016/j.epsl.2018.08.005 (2018).
75 Naafs, B. D. A. *et al.* Introducing global peat-specific temperature and pH calibrations based on brGDGT bacterial lipids. *Geochimica et Cosmochimica Acta* **208**, 285-301, doi:10.1016/j.gca.2017.01.038 (2017).
76 IPCC. IPCC, 2022: Climate Change 2022: Impacts, Adaptation, and Vulnerability. Contribution of Working Group II to the Sixth Assessment Report of the Intergovernmental Panel on Climate Change. (Cambridge University Press. Cambridge University Press, Cambridge, UK and New York, NY, USA, 2022).

Methods

Site descriptions are available in supplementary section 1, file B, and further information in supplementary section A.

Lipid Biomarker Extraction and Characterisation

Bligh and Dyer Extraction

Freeze-dried peat samples were ground to a homogenized powder using a ball mill grinder. Roots and other plant fragments were not removed, in order to ensure a representative sample. Approximately 0.4 g of ground peat was then extracted using a stepwise modified Bligh-Dyer approach.[77,78] The first

extraction was conducted three times using solvent mix A (methanol: dichloromethane: phosphate buffer; 2:1:0.8 v/v; 6.4 mL); the phosphate buffer had a concentration of 9.18 g L^{-1} and a pH 7.4. The sample was vortexed for ~30 seconds and then sonicated in an ultrasonic bath for 15 minutes. Afterwards, the peat and extract were centrifuged at 3000 rpm for 12 minutes, and the supernatant was collected into a new vial. The residual peat was then extracted three times with solvent mix C (methanol: dichloromethane; 2:1 v/v; 6.4 mL), with supernatants again collected after centrifugation. The supernatants were combined and the solvent ratio adjusted to a methanol: dichloromethane: phosphate buffer (or double distilled water) ratio of 1:1:0.9 v/v. The samples were vortexed, and centrifuged (2500 rpm, 10 minutes). The organic layer was collected with a glass pipette and evaporated to dryness under N_2 to obtain a total lipid extract.

Column Separation

The total lipid extract was separated into four fractions through two column chromatography steps: acid and neutral compounds were first separated, and then the latter were separated into aliphatic, aromatic, and polar fractions. First, Isolute NH_2 Bulk 100 Sorbent was added to a glass column (2 cm height) and pre-conditioned with dichloromethane: isopropanol (2:1 v/v; 6 mL). The sample was loaded onto the column and dissolved in a small volume of dichloromethane isopropanol (2:1 v/v). The neutral fraction was eluted using dichloromethane: isopropanol (2:1 v/v; 6 mL), and the acid fraction was then eluted using 6 mL of 3% acetic acid in methanol (v/v). Both fractions were dried under N_2 (40°C). The neutral fraction was separated into aliphatic, aromatic and polar compounds using flash column chromatography. Silica powder (4 cm) was added to a glass column and preconditioned with hexane (2 mL) before a small volume of hexane: dichloromethane (9:1 v/v) was used for sample loading. The aliphatic, aromatic and polar fractions were eluted using hexane (4 mL), hexane: dichloromethane (9:1 v/v; 3 mL), and methanol: dichloromethane (2:1 v/v; 3 mL) respectively. Fractions were then dried under N_2 (40°C).

Urea adduction

Urea adduction was carried out on the neutral aliphatic fraction from samples containing a much higher *n*-alkane concentration than the hopanes and hopenes. Two urea adduction cycles were carried out. For the first cycle, urea in methanol (10 %; 200 µL), acetone (200 µL), and hexane (200 µL) were added to the dried sample, and left in the freezer. After 60 minutes the solvents were removed under nitrogen. The dried crystals were washed three times with *n*-hexane (~ 1mL) and transferred into a vial (containing the non-adductable branched and cyclic alkanes/enes). The urea crystals were dissolved in methanol (500 µL) and double distilled water (500 µL), before adding hexane (~ 1 mL). The sample was vortexed for thorough mixing, and the adductable aliphatic alkanes were extracted three times with *n*-hexane (1 mL). This process was repeated once more on the adductable fraction to ensure that all the non-adducts were removed. These non-adductable fractions were combined and concentrated in a vial.

GC-FID and GC-MS

Aliphatic fractions (or adduct and non-adduct sub-fractions) were diluted with 40 µL ethyl acetate including 2 µL of a prepared androstane standard (0.3 µg/ µL). Aliphatic fractions were first screened

using GC-FID (flame ionization detector) to assess sample quality and concentration; they were injected onto a Trace 1300 Gas Chromatograph in spitless mode at 70 °C, the temperature increased to 130 °C at 20 °C/min for 3 mins, then increased to 320 °C at 5 °C/ min for 47 mins, and then held isothermal for another 24.5 mins. A dimethylpolysiloxane non-polar capillary column (Agilent HP-1, 50 m x 0.320 mm, df 0.17 µm) was used, with helium as the carrier gas at a constant flow of 2 mL/ min.

Aliphatic fractions (or adduct and non-adduct sub-fractions) were analysed via GCMS using a ThermoScientific Trace 1310 gas chromatograph coupled to an ISQ 7000 Quadrupole mass spectrometer. The column and injector were the same as for GC analyses. The oven temperature was set to 70 °C followed by a subsequent ramp of 4 °C /min to 300 °C, where the temperature was held for 24 minutes. Helium was used as carrier gas, with a constant flow rate of 1 ml/min. The mass spectrometer continuously scanned *m/z* 50-650. Instrument performance was monitored using a fatty acid methyl ester (FAME) standard. Hopanes and hopenes (diploptene) were identified based on both mass spectra and retention times. Both the biologically derived R isomer and the diagenetic/geological S isomer of C_{31} 17α(H),21β-homohopane were detected in the new dataset.

GC-IRMS

Short-chain n-alkanes (≤ *n*-C_{19}) had low abundances precluding their carbon isotopic determination. Some samples exhibited co-elution between *n*-alkanes and hopanes or other hydrocarbons and were subject to urea adduction and subsequent silica column cleanup, as described above. Samples for GC-IRMS, therefore, included aliphatic fractions, non-adductable and adductable fractions from urea adduction. For most samples, concentrations were very low; in these cases, the dried fraction was dissolved in 5 µL hexane, and 2 µL were manually injected onto the GC-IRMS. Where autosampler injection was possible, the sample was dissolved in 20 µL of hexane and 1 µL was injected.

Gas chromatography-combustion-isotope ratio mass spectrometry (GC-C-IRMS) was performed using a Thermo Finnigan Delta Plus XP with an Agilent HP-1 column (50 m x 0.320 mm, df 0.17 µm). Samples were measured in duplicate (and the average value reported) and $\delta^{13}C$ values were converted to Vienna Pee Dee Belemnite (VPDB) notation by calibrating against an in-house reference CO_2 gas of known $\delta^{13}C$ value. Monitoring of the instrument stability was carried out through analysis of a six-component FAME (fatty acid methyl ester) isotope reference mixture after every two samples (4 injections), with an analytical precision of ±0.5‰. Averages and standard deviations were calculated based on the duplicate runs, and based on variations from the FAME standard.

For the C_{31} αβ hopane, both the R and S isomers were integrated separately, although the latter was typically less than 10% of the total. Previous papers have reported solely $\delta^{13}C$ values of the C_{31} αβ hopane-22R isomer, although the S isomer was likely present in those as well.

Bulk Organic Carbon Isotope Determination

Dried, homogenised peat was weighed (~0.5 to 1 mg) into tin capsules. Analysis included the elemental C and N contents and $\delta^{15}N$ and $\delta^{13}C$ stable isotopes via a continuous flow isotope ratio mass spectrometer (Elementar Isoprime Precision; Elementar Analysensysteme GmbH, Hanau, Germany)

coupled with an elemental analyser (EA) inlet (vario PYRO cube; Elementar Analysensysteme GmbH, Hanau, Germany), as described by *Sgouridis et al., 2023 (section 2.2)*. Briefly, the EA was calibrated with sulfanilamide (N: 16.26 %, C:41.81 %, S: 18.62 %) and the precision as a RSD was <5% for both C and N. The IRMS was calibrated against international reference standards (caffeine: USGS61 (−2.87 ‰ δ^{15}N, −35.05‰ δ^{13}C VPDB), USGS62 (20.17‰ δ^{15}N, −14.79‰ δ^{13}C VPDB), USGS63 (37.83 ‰ δ^{15}N, −1.17‰ δ^{13}C VPDB) and the precision as a standard deviation (SD) was < 0.06‰ for both δ^{15}N and δ^{13}C stable isotopes.[79]

Microbiology

Microbiological data from Panama have been previously reported,[80] although they were only briefly discussed, with no consideration of methanotroph community structure and have been reprocessed through the same pipeline for this study. For sites new to this dataset, i.e the three Colombian sites, the Uganda Papyrus Swamp, and British Ombrotophic Bog, microbial community was analysed using microbial genomic DNA extraction and sequencing of 16S rRNA genes. Note: that the Tor Royal analyses were conducted on a different suite of cores than those used for biomarker analyses. After being stored in buffer, 400 mg of subsampled wet peat was community extracted using DNeasy® PowerSoil® Pro kit (Qiagen, Germany) following the provided protocol. The extract was eluted using Tris-HCl (10mM) before the concentration was measured using 1X dsDNA HS assay kit on a Qubit™4 fluorometer (Invitrogen). The extract (30 µL) was sent to Novogene (Novogene UK Ltd., Cambridge), for 16S sequencing (V4 region) using polymerase chain reaction (PCR) techniques. Primers used were 515F (TGCCAGCMGCCGCGGTAA) and 806R (GGACTACHVGGGTWTCTAAT). All the old and new raw data were processed using the DADA2 pipeline Version 1.34.0[81] in R Version 4.4.3 to obtain amplicon sequence variants (ASVs), before being given taxonomic assignments based on Silvia 138.1 database.[82] Further analysis was carried out using data created into a phyloseq object using the package 'phyloseq' Version 1.50.0.

Data Availability

Sequencing data of the Cananguchal (CAC), Pantano (CAP) and Tor Royal (UKTR_1) samples generated in this study have been deposited in the NCBI Sequence Read Archive under BioProject accession number PRJNA1511607.

Sequencing data of the Uganda Mpologoma Swamp Point A (UMS_PA) samples generated in this study have been deposited in the NCBI Sequence Read Archive under BioProject accession number PRJNA1511655.

Sequencing data of the Panama and Everglades samples generated in this study have been deposited in the NCBI Sequence Read Archive under BioProject accession number PRJNA1356914. Link https://dataview.ncbi.nlm.nih.gov/object/PRJNA1356914?reviewer=4lsdbj3ckjb3g1gl4e0np2rl7u

References:

77 Wörmer, L., Lipp, J. S. & Hinrichs, K.-U. in *Hydrocarbon and Lipid Microbiology Protocols Springer Protocols Handbooks* Ch. Chapter 183, 289-317 (2015).

78 Bligh, E. G. & Dyer, W. J. A Rapid Method of Total Lipid Extraction and Purification. *Canandian Journal of Biochemistry and Physiology* **37**, 911-917 (1959).
79 Sgouridis, F. *et al.* Stimulation of soil gross nitrogen transformations and nitrous oxide emission under Free air CO2 enrichment in a mature temperate oak forest at BIFoR-FACE. *Soil Biology and Biochemistry* **184**, doi:10.1016/j.soilbio.2023.109072 (2023).
80 Schneider, V. *et al.* Environmental indications and controls of bacterial membrane lipids in a tropical peatland from Panama. *Organic Geochemistry* **210**, doi:10.1016/j.orggeochem.2025.105094 (2025).
81 Callahan, B. J. *et al.* DADA2: High-resolution sample inference from Illumina amplicon data. *Nat Methods* **13**, 581-583, doi:10.1038/nmeth.3869 (2016).
82 McLaren, M. R. & Callahan, B. J. Silva 138.1 prokaryotic SSU taxonomic training data formatted for DADA2 [Data set]. *Zenodo*, doi:https://doi.org/10.5281/zenodo.4587955 (2021).

Acknowledgements

The authors acknowledge the people involved in management of these peatlands including Natural England, PNN Amacayacu, Smithsonian Tropical Research Institute, Wetlands Management Department, Ticuna, Miccosukee, Seminole, and Caño Vitina.

Author contributions

R.D.P and M.N.J conceptualised the study; fieldwork was carried out and supported by A.O., M.N.J., MV., S.M.K.C., A.V.G.S., C.B., Y.Z., F.K., C.K., E.K., J.C.B., D.P.A.P; lab work was conducted by M.N.J., M.V., A.O., A.A., and D.P.A.P; project was administered by R.D.P., A.V.G.S., C.B., and B.D.A.N; original draft was written by M.N.J., and R.D.P., and reviewing and editing was carried out by all co-authors.

Funding statement

M.N. Jenkins, R.D. Pancost, C. Bryce, A.V. Gallego-Sala, B.D.A. Naafs, and Y. Zhang acknowledge funding from the Leverhulme Trust [BACC RPG-2022-245]. M. Vreeken is funded through PhD studentships at the Great Western Alliance Doctoral Training Partnership (NERC GW4+ DTP2) [NE/S007504/1]. R.D. Pancost, C. Bryce, A.V. Gallego-Sala, B.D.A. Naafs, A. Oakeshott, T.A. Halamka, and S.M.K. Cheung acknowledge funding from UK Research and Innovation (UKRI) under the UK government's Horizon Europe funding guarantee [CERES EP/X023214/1]. Juan C. Benavides and D.P. Alarcon Prado acknowledge funding by the National Academies of Sciences, Engineering, and Medicine under the PEER program (grant code 9-166). B.D.A. Naafs also acknowledges funding through a Royal Society Tata University Research Fellowship. A.V. Gallego-Sala acknowledges funding from the European Research Council (ERC) under the European Union's Horizon 2020 research and innovation programme (grant agreement no. 865403). A.A. was supported by a University of Exeter Sanctuary Scholarship, with data also funded by ERC under grant agreement No. 865403. C.S.-M. and A.V.G.-S. also acknowledge support from TROPWET, an NSF–NERC joint award (NSF 23-549; NE/Z000246/1). The authors also wish to thank the NERC for partial funding of the National Environmental Isotope Facility (NEIF; contract no. NE/V003917/1).

Competing Interests

The authors declare no competing interests.

Additional Information

Supplementary information and raw data available.

Supplementary Files

This is a list of supplementary files associated with this preprint. Click to download.

- SupplementaryInformationA.xlsx
- PeatlandclimatemethanefeedbacksinwarmingperiodsweregovernedbypHandhydrologySIB.docx